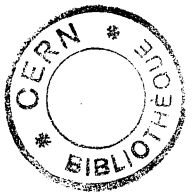

LYCEN/8670
Novembre 1986

PERFORMANCES OF LARGE BGO CRYSTALS BELOW 20 MeV

BURQ J.P., CHEMARIN M., EL MAMOUNI H., HE J.T.[1], FAY J., GOYOT M., ILLE B., JACQUET G., LAMBERT M., LEBRUN P., LU Y.S.[1,2], MADJAR N., MAURELLI G., MARTIN J.P., REYNAUD M., SAHUC P., TUNG K.L.[1,2]

Institut de Physique Nucléaire (and IN2P3), Université Claude Bernard Lyon-1
43, Bd du 11 Novembre 1918 - 69622 Villeurbanne Cedex, France

ABSTRACT

This paper presents the performances of large tapered BGO crystals to low energy photons of 6 to 20 MeV. The read-out of the crystals was made with large area photodiodes associated to shaping amplifiers.

(1) Permanent address : *Institute of High Energy Physics Beijing, China*

(2) Supported in part by *CERN, CH-1211 Geneva-23, Switzerland*

1. INTRODUCTION

The electromagnetic calorimeter of the L3 experiment at LEP will be built using a fine grained barrel of large BGO scintillators pointing to the interaction region. It will consist of about 12000 24 cm long, tapered BGO crystals. Being located in a region of 5 Kgauss magnetic field, the scintillators will be instrumented with 2 photodiodes of 1.5 cm^2 active area each [1].

Because photodiodes have no gain an electronic amplification of high gain is required. As a consequence the signal/noise ratio is worse than in case of photomultiplier tubes read-out and detecting low energy particles with BGO is not easy as it is sketched in figure 1 with a 6 Mev gamma ray.

In this paper we report on results obtained with a 3*3 BGO crystals matrix detecting gammas of energy below 20 Mev. The present work has been undertaken to measure the response of large BGO modules to low energy gamma in view of investigating a method to monitor and even to calibrate "in situ" the electromagnetic calorimeter by mean of radiative capture radiations. Such a method , which has been already used in the SLAC Crystal Ball experiment , is forseen to be applied in the L3 experiment together with other methods such as cosmic rays detection in conjonction with Xenon lamp monitors.

The system of nine BGO modules , which have almost the final geometry, was tested with 6 to 20 Mev gamma rays at the 4 Mev protons Van de Graaff of the Lyon Nuclear Physics Institute.

After a short description of the experimental setup and the BGO matrix with its associated electronics is made (section II), the matrix characteristics (noise, intercalibration, light conversion) are presented in section III and the beam results are summarized in section IV with a comparison with EGS data. Finally a summary is given in section V.

2. THE EXPERIMENTAL SETUP

1) The Van de Graaff layout

The experimental layout is shown in figure 2. Monochromatic photons of 6.13 Mev to 20 Mev were provided by a 4 Mev protons Van de Graaff using (p,γ) reactions. Two different targets were bombarded by a HH^+ beam at different incident energies :

– a home-made 160 $\mu g/cm^2$ LiF target , 33 Kev thick, deposited on a tantalum support

– a 320 Kev thick tritium target made of tritium absorbed in a titanium layer on a 0.5 mm thick tantalum backing [2]. The activity of this target was 5.4 Ci spread over a 25.4 mm diameter area (3.35 Ci/cm^2). This target necessitated of course an appropriate safety monitoring system to prevent for any tritium leakage. In order to avoid the accelerator contamination the target was continuously water-cooled and in addition a thin Nickel foil, 2 μm thick, isolated the reaction chamber from the accelerator beam pipe.

Table I summarizes the protons radiative capture reactions which produce the gamma rays we needed for our study. The reaction on Fluor is very convenient because of the abundant production of a clean sharp 6.13 Mev line. The reaction with Lithium gives also a sharp 17.6 Mev peak which is unfortunatly disturbed by the presence of a broad 14.8 Mev resonance. Because the LiF target was thin, it was possible by tuning the beam energy, to select the gamma lines. The last reaction, despite its anisotropy and its small cross section, is interesting because it produces an isolated gamma line, the energy of which increases with the incident proton energy. We restrict ourselves to protons kinetic energy just below 1.02 Mev because of the very abundant neutrons production coming from the ^3H $(p,n)^3He$ reaction which occurs above this energy threshold

A 4″*6″ NaI crystal surrounded by a lead shielding was installed to monitor the beam conditions and the nuclear reactions. The NaI pulse height distributions shown in figure 3 correspond to the different experimental conditions of table I.

The beam intensity was typically 2 to 4 μA with the LiF target and 0.2 to 0.4 μA with the tritium target in order not to destroy the Ni foil.

2) The BGO matrix

The detector assembly, shown in figure 4, consisted of nine tapered BGO crystals, each 20*30*240 mm^3, constructed in a 3*3 crystal matrix in such a way the central crystal axis was horizontal and pointed to the target center. The nine crystals were taken among the first ones supplied by the Shanghai Institute of Ceramics [3]. The non-uniformity of the crystals response along their axis, which was due to their pyramidal shape, has been corrected by depolishing two lateral faces [4] (all the other faces being optically polished) and wrapping the crystals in a thin, white painted Aluminium foil (NE 560 paint from Nuclear Entreprise). Figure 5 shows typical examples of longitudinal uniformity measured with either a ^{137}Cs or a ^{60}Co gamma source and a photomultiplier for two crystals and two different wrapping conditions. For the nine crystals the non-uniformity has been found to be less than ± 3 % over more than 90 % of their length. The FWHM energy resolution for the 0.66 Mev gamma ray of the ^{137}Cs source, measured with a photomultiplier and a NE 560 painted reflective foil goes from 22 % to 27%, depending on the crystal.

The crystals and the front-end electronics (charge sensitive preamplifiers) were encased in a light-tight brass box for shielding as shown in figure 4. The room temperature was 18^0 C. No thermal stabilization was achieved but the temperature fluctuations in the Van de Graaff experimental area during the data taking were less than ± 1^0 C .

Figures 6 and 7 show the crystal arrangement viewed from the entrance face ; S59 was the central crystal of the matrix. The distance between the matrix front face and the target was 50 cm.

A great attention was paid to protect the BGO crystals against the daylight which was shown to deteriorate the crystals transmission ; any crystal handling has been made in the darkness or yellow light.

3) The photodiodes and their associated electronics

Three S1790 "windowless" Hamamatsu photodiodes (1 cm^2) were cemented to the rear face of each crystal with Dow Corning 3145 RTV and connected in parallel with each other. The area around the photodiodes was painted with usual typing correction fluid to enhance the light collection efficiency.

The diodes reverse bias was 12 volts. Their average capacitance at this bias value is about 85 pf. On average the three photodiodes assembly leakage current at 12 volts was about 2.1 nA, that is 0.7 nA for each photodiode. Two years after being glued on the crystals their leakage current has been found to be very stable apart one of them showing an abnormally high reverse current (several μA at 10 volts ; this diode has been changed).

The hybridized, 1"*4/5" , low noise charge sensitive preamplifiers (CPA) have been described in detail elsewhere [5]. Their input stage uses the 2SK 147 BL FET from Toshiba which is well adapted to detectors with large capacitance (about 250 pf in our case). The main characteristics of the CPA's are extensively discussed in ref [5,6] .

The CPA's were connected to the photodiodes via short non coaxial cables (about 5 cm long) . The photodiode-CPA coupling was of AC type. An Aluminium foil shield protected each module (= the CPA-photodiodes combination) as shown in figure 4 in order to avoid cross-talk.

The CPA's output pulses (300 ns rise-time , which is the BGO scintillation decay-time , and 1 ms decay-time) were sent via three meters coaxial cables to RC-CR shaping amplifiers whose outputs were fed to two 11 bits commercial CAMAC ADC's (Ortec AD 811 and LRS 2259B). We used both commercial Ortec 572 shaping amplifiers (in particuliar for the central crystal) and home-made shaping amplifiers. The filtering constant was 2 μs , which was almost the optimum value from the signal/noise ratio point of view.

4) Data Acquisition

The CAMAC acquisition was performed by either a VME 10 or a HP 2100 on-line computer and the ADC data were recorded on magnetic tape. One problem we had to solve, because of the continuous Van de Graaff beam, was to build a triggering signal. It was obtained by coupling a photomultiplier tube to the central crystal as shown in figure 4 and figure 7. A one cm diameter aperture was done in the wrapping of the crystal front face, allowing a small fraction of scintillation light to be detected by the photomultiplier. It has been measured , with the help of a gamma source and a photomultiplier, that the loss of collected light due to such a hole in the front face wrapping is of the order of 1 % to 2 % maximum, without having any effect on the response uniformity. This triggering

technique has therefore negligeable consequence on the crystal performance . It is to be noted also that such a trigger selected photons arriving in majority everywhere on the central crystal front face (the incoming photons were not collimated).

3. MATRIX CHARACTERISTICS

Great care was taken to characterize the BGO modules of the matrix, specially the electronic noise and the light conversion which are the main parameters governing the detector performances at such low energies :

i) A high precision Ortec 448 research pulser injecting calibrated charges on a 1 pf ± 0.05 pf test capacitance located at the CPA input (figure 2) was used to determine the gain and to control the whole electronic chain linearity and stability. The gain of each channel is presented in the second column of table II. The large dispersion in the gain came mainly from the amplifiers which were of different types : channel 3,4,5 and 6 were instrumented with Ortec amplifiers whereas the other channels were instrumented with home-made amplifiers having a lower gain.

ii) The calibration of the central module and the intercalibration of the BGO crystals of the matrix were performed using cosmic ray data. The cosmic rays were selected by mean of two 3 cm wide, 30 cm long scintillators placed on each side (top and bottom) of the crystals assembly , as shown in figures 4 and 6. The data were recorded on magnetic tapes and a more severe selection was made off-line by requiring that each crystal of a same column detected at least 40 % of the average deposited cosmic ray energy in the crystal (see figure 6) in order to reject too much inclined tracks. An example of cosmic ray energy spectrum is shown in figure 8 : the absolute calibration constant of the central crystal , assuming 9 Mev per BGO cm for minimum ionizing particles , was 19.1 Kev/ADC channel (with an estimated uncertainty of 2 to 4%, mainly due to the geometry). Next the comparison of the energy distribution of the other crystals with the central one determined the intercalibration constants to within 1 % (third column of table II).

Then the knowledge of the electronic gain of each channel allows the extraction of the relative "intrinsic" efficiency of each crystal : these efficiencies are shown in the fourth column of table III. These numbers reflect all the contributions which governed the light yield converted in the photodiodes : scintillation and wrapping efficiencies, crystal transmision and coupling transmission. The photodiodes quantum efficiency did not contribute significantly to this dispersion. It has been shown, with the help of a blue led's generator ($\lambda = 490$ nm) illuminating via an optical fiber a sampling of "windowless" S1790 photodiodes , there were negligeable differences in the photodiodes responses. This is shown in figure 9 which shows some photodiodes responses (CPA output) to blue led's excitations before and after gluing : the dispersion is 1 % maximum. As it can be seen in the table the "intrinsic" efficiency of the crystals varied at most by 40 % (crystals S57 and S66).

iii) The conversion factor of the BGO crystals, that we can define as the number of photoelectrons per deposited unit energy, has been determined to within a few percents by comparing the electric pulser signals (=injected electrons per ADC channel) with the cosmic ray peaks (=deposited energy per ADC channel). These factors are quoted in the sixth column of table II : on average we obtained 330 electrons per one Mev deposited and for a light collecting area of 1 cm^2.

iv) The electronic noise was our main concern. It has been determined by several independant methods which we will describe shortly here :

The first method used the precise electric pulse test generator mentioned above which injected known charges on the CPA test capacitance.

A second method consisted to use a led's generator illuminating the front face of the crystals via 2 meters plastic optical fibers (except the central crystal because of the PM coupling). This generator presented the advantage to check at the same time the crystal transmission, the photodiodes-CPA's functionning and their couplings to the crystals . Moreover it was well adapted to electronic noise determination because it avoided electric couplings which were susceptible to generate parasitic correlated noise (no connection between the crystals assembly and the electronics).

Both pulse and light test generator data were recorded on magnetic tapes during special runs performed before and after each beam data taking. The light generator was calibrated with the help of the electric pulse test generator.

An other interesting method consisted to use a low energy gamma source. In our case, we used a ^{57}Co source, located on the CPA's board as it is shown in figure 4. The two gamma lines delivered by the source (122.06 Kev and 136.47 Kev) were directly detected in the photodiodes which acted as nuclear detectors. A typical example of ^{57}Co energy spectrum obtained with the central module is shown in figure 10 : the two gamma peaks are clearly separated from the electronic background (which appears in the lowest channels) and the physical background (Compton scattering and backscattering). This method has the advantage to be an absolute measurement in electrons of the electronic noise , if we take into account that 3.6 ev are needed on average to create an electron-hole pair in silicon at room temperature. This method which checked also directly the whole crystal front-end electronics was applied during the matrix preparation and after the data taking. It can be used also to measure the injection test capacitance of the CPA's.

In addition a random generator was used essentially to determine the pedestal values and to verify their stability. Because of a small non linearity of the ADC in the lowest channels, the pedestals were a little bit distorted (non gaussian-like shape). As a consequence their widths were underestimated by about 20% to 30%, depending on the ADC inputs. The pedestal peak value of the nine channels did not change by more than $\pm$ 1 channel.

These noise determinations are summarized in figure 11 which shows the light and electronic test generators results versus the independant ^{57}Co source noise data. As we can see in this plot, whereas the led's and the electric pulser data were about the same, the source noise estimations were systematically greater than the two others by a factor 1.2 on average. Collection effects in the whole 100 μm thick silicon layer were probably responsible for this difference. For this reason we thought the source data overestimated the pure electronic noise contributions and we took for granted the generators values which are quoted in the fifth column of table II : these numbers in units of electrons, express an inherent photodiode-CPA-amplifier characteristic. On average the electronic noise level per module was about 1000 electrons.

It is interesting to remark that part of this noise was correlated. This has been demonstrated with the test generators data by calculating the whole BGO matrix noise in two different ways :

– first, by computing the quadratic sum QS of the nine channel noises (SIG(QS) = $\sqrt{\Sigma\ \sigma^2}$)

– second, by considering the r.m.s. of the Σ_9 distribution obtained by adding the nine channels of the matrix (SIG(Σ_9))

The SIG(Σ_9)/SIG(QS) ratio was about 1.2 which indicates the presence of a correlated contribution to the noise of the order of 20% for the complete 3*3 matrix.

Finally the matrix characteristics can be summarized in the two last columns of table III. They show the main parameters which are responsible for the signal/noise ratio : the seventh column represents the signal delivered by each module when one Mev is absorbed in it (this quantity is directly related with the quality of the detection system) whereas the final column contains the noise of each channel in Mev-BGO unit reflecting both the front-end electronics and the detection system performances. These noises cluster around 1.0 Mev and range from 0.8 to 1.7 Mev. This is the main contribution to the energy resolution below 20 Mev.

4. VAN DE GRAAFF RESULTS

Because of the triggering technique applied, the crystal with the largest energy was most of time the central one. A lot of events were issued from spurious triggers due to the PM noise and consequently gave nothing in the central crystal (pedestals population). This is illustrated in figure 12 showing raw correlations between the central channel and a neighbouring one : figure 12a corresponds to 6 Mev gammas, figure 12b corresponds to 6 and 14-17 Mev gammas. As it can be seen in this figure (at least for energies above 6 Mev, figure 12b) the photon energy is not completely deposited in the central crystal.

A simple data analysis that consisted to use the crystals surrounding the central one as vetoes has been performed. Each event giving an energy signal above a certain threshold in one of the eight surrounding crystals was excluded in the central energy distribution. However an attempt to add several channels has been made at the highest available energy (= 20 Mev and only at this energy because of the noise level per channel) in order to see the summation effect on the energy resolution.

The experimental central energy distributions are shown in figure 13 to 16. For each energy, several distributions corresponding to different vetoing conditions are presented : no cut at all, a two sigmas cut and a 0.5 sigma cut respectively (that is to say about 2 Mev and 0.5 Mev energy cuts on the neighbours). The 14.8 Mev and 17.6 Mev peaks cannot be resolved (figures 14 and 15) even with the most severe cut. Figure 15, corresponding to the beam conditions where the $^{19}F(p,\gamma)\ ^{16}O$ and the $^{7}Li(p,\gamma)^{8}Be$ reactions were in competition, shows clearly the sharp 6 Mev line and the broad 14-17 Mev distribution. Figure 16 shows the isolated 20 Mev peak which is unfortunatly accompaned by an important physical background produced mainly in the target backing and the target support (the 20 Mev gammas counting rate was very low, about 2 to 3 events/s). For example the 4.4 Mev peak from the ^{12}C first excited state is clearly apparent.

Apart the 6 Mev distribution, all the other spectra have a non-gaussian shape, with a lower part and a peak value depending on the veto cuts and the physical background. We concentred on the front edge determination, in particular the upper half height value of the peak (HH^+) which turned out to be the most stable parameter with respect to the vetoing conditions. For the 17.6 and 20 Mev spectra, both the peak and the HH^+ values have been obtained by fitting the distribution front edge with either a gauss function or a non-symmetrical "shower-like" function [7] , as it is illustrated in figure 17. With the statistics available , these two kinds of HH^+ determinations agreed within 1%. Owing to the non-gaussian shape of most of the spectra, the resolution σ/E is defined as the FWHM/2.36/peak or even better as the Δ^+/peak where Δ^+ is the upper half width at half height of the peak (in case of a gaussian shape Δ^+ overestimates the true sigma by a factor 1.15). These results are quoted in tables III to V : the energy scale comes from the cosmic rays calibration of the central channel. We see the HH^+ values are independant of the veto cuts within our level of accuracy. The experimental resolution σ/E of the central crystal goes from about 20% at 6 Mev independantly of the veto cut to about 9% and 6% at 20 Mev respectively for a two sigmas and 0.5 sigma veto cut (figure 18 ; the solid line curve represents the 0.8/E electronic noise contribution).

A Monte Carlo simulation of the 3*3 tapered crystals matrix using EGS4 [8] has been carried out. The electronic noise has been taken into account by convoluating the simulated EGS4 energy with gaussian distributions whose sigmas were the measured values (0.8 Mev for the central crystal).

The ECUT and PCUT thresholds were 0.6 Mev and 0.010 Mev respectively. An example of such a simulated distribution for a 20 Mev gamma ray is shown in figure 19. In order to compare the experimental results with the Monte Carlo simulation the same analysis we made for the experimental data has been applied to the EGS spectra. The results are summarized in the tables III to V together with the experimental data.

A correlation plot of the simulated and the experimental data is presented in figure 20. Both the peak and the HH^+ values are distributed along a straight line whose slope is almost 1.0 . A finer analysis, though, shows a correction of 1.5% has to be applied on the cosmic rays calibration constant which becomes 18.8 Kev/ADC channel. This correction could be due either to the value of the minimum ionizing energy loss in BGO we have taken or to a systematic error in the positioning of the central crystal with respect to the cosmic rays scintillators. Moreover the pedestal value of the central channel seems to be overestimated by about 10%; this is due to the non linearity effects of the ADC's already mentioned.

The figures 21 show examples of 20 Mev gamma line distributions obtained by adding the highest energy crystals (from 2 to 5 in the fig.). The shape of the peak is becoming gaussian but the energy resolution is appreciably deteriorated (13% to 17% compare to $\leq$ 9% in case of the central crystal alone) as it is shown in figure 22 which is a plot of Δ^+/peak versus the highest energy crystals number . Obviously this worsening of the resolution is mainly due to the electronic noise which is the most preponderant contribution at these low energies. Summing several channels did not ameliorate the energy resolution.

Radiation damage measurements have been carried out with the BGO assembly as an application of our monitoring method . A small volume of the central crystal (of about 2*2*3 cm^3) situated at the end away the readout has been uniformely exposed to 18 Mev photons delivered by the electrons accelerator of the Lyon Anti-Cancer Hospital . The irradiation has been performed in two steps : the first one corresponded to a 120 R dose and the next step was a 600 R exposure of the same volume four days later . The radiation effects have been monitored by comparing the peaks positions of the 6 and 14-17 Mev photons before and two hours after irradiation . For the 120 R dose , an effect of -5 % has been observed for the two peaks with a recovery of about $+1.3$ % 24 hours later. For

the 600 R dose , an effect of -17 % has been measured with a recovery of $+5$ to $+6$ % 24 hours later . The radiation damage effects were monitored identically (within our accuracy) by the 6 Mev and 17 Mev gamma . In L3 , the radiation expected in normal operation is less than 1 R/day everywhere on the BGO calorimeter ; but it could be $\approx$ 60 R in the endcaps and $\approx$ 2400 R in the forward detectors in case of accidental beam loss [1] .

5. CONCLUSION

An assembly of nine large BGO crystals equipped with large area silicon photodiodes has been tested at low photons energies . The crystals manufactured by the Shanghai Institute of Ceramics were wrapped in a NE 560 painted Al foil . They were uniformized by depolishing two of the four lateral faces and coupled to three S1790 , 1 cm^2 , Hamamatsu photodiode with Dow Corning 3145 RTV glue . In these conditions , the light conversion factor was 330 e^-/ cm^2 sensitive area/ Mev on average and the noise level of the 3*1 cm^2 photodiodes-charge sensitive preamplifier combination was typically 1000 e^- ($\approx$ 1 Mev BGO) . The measurements reported here showed a satisfactory detection of photons in the range 6 to 20 Mev . At such low energies the electronic noise is the main limitation to the energy resolution . At 6 Mev the energy resolution (FWHM/2.36/peak) measured with the central crystal is 20 % , independantly of the vetoing conditions adopted on the surrounding crystals . At 20 Mev the veto crystals killed effectively escapes and the peak shape depends on the energy cut-off . The energy resolution (Δ^+/peak) goes from 6 % to 9 % for an energy cut-off ranging from respectively 0.5 Mev to 2 Mev . Because of the electronic noise contribution , summing several crystals deteriorates the energy resolution up to 13 $\div$ 17 % .

Good agreement was found between our three energy data and a simple EGS simulation . Although more work has to be done , these results give us confidence in using such a method for "in situ " calibration purpose . Monitoring radiation effects of a few tens Rad will be easily achievable by mean of low energy gammas . In particuliar the role of the ^{19}F (p,$\alpha\gamma$) ^{16}O radiative capture reaction was shown to be very important in these tests : the sharp , intense 6.13 Mev line was our best energy reference .

Acknowledgments

We would like to thank M. Ferrari , A. Gardon , P. Maissiat , and S. Vanzetto for their skill and cooperation in running the 4 Mev Lyon Van de Graaff facility . We also greatly appreciate the contributions of J.P. Manin who was responsible for the tritium target and safety monitor . We would like to acknowledge Doctor Duthou and Miss Ginestet for their collaboration and their hospitality in the Accelerator Department of the " Centre Léon Bérard " in Lyon .

6. REFERENCES

1) Technical proposal of the L3 experiment (May 83) and Addendum to the L3 technical proposal (April 85).

2) TIT 2C target from the "Centre d'études de Valduc / CEA ", France.

3) Crystals # S57,S58,S59,S61,S63,S65,S66,S67,S68 supplied by the Shanghai Institute of Ceramics delivered in the beginning of 1984.

4) The non-uniformity correction study and the surfaces roughening were developed and performed in the "Laboratoire de Physique des Particules d' Annecy " , LAPP, France.

5) L3-CPA for photodiodes read-out.

M. Goyot IPN Lyon Internal report and L3-BGO report.

6) Performances of preamplifier-silicon photodiode readout system associated with large BGO crystals scintillators .

M. Goyot, B. Ille, P. Lebrun, J.P. Martin " third Pisa meeting on Advanced Detectors ", June 1986, and LYCEN 8663 .

7) Radiative decays of the Psi Prime to all-photon final states.

Roger Alan Lee : SLAC Report 282 (May 1985)

8) The EGS Code System.

Richard L. Ford and Walter R. Nelson : SLAC Report 210 (June 1978) and EGS4 Version of EGS : W. R. Nelson, H. Hiramaya, D. Rogers

7. TABLE CAPTIONS

1) List of (p,γ) reactions used in the tests.

2) Summary table of the BGO crystals characteristics (channel #5 is the central one of the matrix).

3) 6.13 Mev line : experimental results and EGS simulation.

4) 17.6 Mev line : experimental results and EGS simulation . The peak and resolution of the experimental 17.6 Mev line cannot be accuratly defined because of the presence of the 14.8 Mev broad resonance which was not introduced in our EGS simulation.

5) 20 Mev line : experimental results and EGS simulation . The Σ_9 and the Σ_5 (= crystals #2,4,5,6,8 summation , "cross geometry") results are also shown in this table.

Reactions	Gamma rays energy (MeV)	Proton Energy (Kev)
$^{19}F\ (p,\gamma)\ ^{16}O$	6.13 , sharp	650. } 540. both reactions
$^{7}Li\ (p,\gamma)\ ^{8}Be$	14.8 , broad 17.5 , sharp	475. } 540. both reactions
$^{3}H\ (p,\gamma)\ ^{4}He$	20.5 , sharp	1200.0 (Ni foil)

TABLE I : (p,γ) reactions used

chan/cryst.	elect.gain ADC ch./ (mV)	interc. const.	intrins. eff.	el. noise (σ) (elect.)	conv. e/MeV /cm^2	3 pd's signal e/MeV	noise MeV-BGO (σ)
1 / S58	177.0	2.12	0.81	1444.	280.	840.	1.70
2 / S57	180.6	1.38	1.23	1070.	420.	1260.	0.85
3 / S63	198.7	1.36	1.12	1180.	380.	1140.	1.03
4/ S61	305.8	1.07	0.94	890.	325.	975.	0.90
5 / S59	305.3	1.00	1.00	825.	350.	1050.	0.80
6 / S68	295.5	1.02	1.00	840.	350.	1050.	0.80
7 / S65	120.1	2.93	0.88	850.	305.	915.	0.93
8 / S67	212.0	1.57	0.91	1117.	315.	945.	1.18
9 / S66	131.6	3.22	0.71	965.	245.	735.	1.30
MATRIX	average		0.96	1020.	330.	990.	1.05
	dispersion		0.16	205.	52.	157.	0.29

TABLE II : Summary of the characteristics of the BGO assembly

Conditions		Peak (MeV)	HH^+ (MeV)	Δ^+/peak (%)	Γ/2.36 * peak (%)
Experimental	Central	5.25	6.35	20.9	18.2
	2σ cut	5.25	6.35	20.9	18.2
	0.5σ cut	5.25	6.35	20.9	18.2
EGS	Central	5.30	6.35	19.8	19.1
	2σ cut	5.50	6.50	18.2	17.7
	0.5σ cut	5.50	6.55	19.0	15.4

TABLE III : 6 MeV

Conditions		Peak (MeV)	HH^+ (MeV)	Δ^+/peak (%)	Γ/2.36 * peak (%)
Experimental	Central	-	17.7	-	-
	2σ cut	-	17.8	-	-
	0.5σ cut	~16.3	17.7	~8.6 %	-
EGS	Central	16.0	17.6	9.4	12.7
	2σ cut	16.4	17.7	7.9	8.8
	0.5σ cut	16.65	17.75	6.9	5.1

TABLE IV : 17.6 MeV

Conditions		Peak	HH^+ (MeV)	$\frac{\Delta^+}{\text{peak}}$ (%)	$\frac{\Gamma}{2.36 * \text{peak}}$ (%)
Experimental	Central	-	-	-	-
	2σ cut	18.9	20.55	8.8	10.8
	1σ cut	19.1	20.70	8.4	9.1
	0.5σ cut	19.35	20.55	6.2	7.0
	Σ_9	19.1	22.35	17.1	16.8
	Σ_5	18.6	21.2	13.9	14.8
	"cross geom."				
EGS	Central	18.2	20.12	11.0	13.9
	2σ cut	19.3	20.45	6.0	9.1
	Σ_9	19.8	22.44	13.4	12.5
	Σ_5	19.5	21.6	10.8	11.6
	"cross geom."				

TABLE V : 20 MeV

8. FIGURE CAPTIONS

1) Pulse height distribution of a Pu-C gamma source (6.13 Mev line):

1a) The source was placed in front of a 2*3*24 cm^3 BGO crystal from Harshaw at room temperature. Three S 1790.01 "windowless" Hamamatsu photodiodes were glued on the rear face of the crystal for light conversion. The wrapping was from Harshaw Chemical Company. All the faces of this tapered crystal were optically polished.

1b) Direct energy spectrum of the source obtained by connecting the photodiodes #1 and #2 in parallel to a charge sensitive preamplifier whose output pulse was amplified in a standard shaping amplifier . The 6 Mev peak appears only as a shoulder above the electronic noise.

1c) Same spectrum as in figure 1b, but photodiode #3 was in coincidence (inhibit input of the Nucleus multichannel analyzer). The coincidence removes part of the electronic noise and the 6 Mev gamma line appears now clearly above the noise. The peak value is at about 5.6 Mev (the escape peaks cannot be resolved).

2) The Van de Graaff general layout. In order to have a stable operating of the accelerator for proton energy below 1 Mev it was better to accelerate a HH^+ beam. When the LiF target is in use, the Ni foil is removed and the BGO matrix is aligned with the beam direction.

3) The NaI beam monitoring energy spectra for different operating beam energy :

3a) the 6.13 Mev gammas with the single and double escape peaks (HH^+ beam energy = 1.3 Mev)

3b) upper part of the previous spectrum showing the presence of 14.8 and 17.6 Mev lines

3c) the 14.8 and 17.6 Mev lines. The 6 Mev peak is still present because of the strong $^{20}Ne \rightarrow {}^{16}O + \alpha$ transition (HH^+ beam energy = 0.95 Mev)

3d) the 6.13 Mev / 17.6 Mev peaks proportion can be changed by varying the beam energy (HH^+ beam energy = 1.0 Mev ; about the same proportion in this case)

3e) the ^{4}He 20 Mev peak with cosmic rays (HH^+ beam energy = 2.4 Mev ; because of the energy loss of the incident proton in the Ni foil we are still below the neutron production threshold). Due to the multiple Coulomb scattering of the protons in the foil, the beam spot covered the whole target surface.

4) Transverse view of the BGO assembly.

5) Longitudinal uniformity of crystals # S59 and S61. Using NE 560 paint instead of white paper enhances the light collection by about 17% and ameliorates the response uniformity. Here the origin of the x-axis corresponds to the PM location (3*3 cm^2 downstream face).

6) Location of the crystals in the matrix.

7) Perspective schematic view showing the matrix arrangement.

8) Cosmic ray energy spectrum in the central crystal.

9) Some S1790 Hamamatsu "windowless" photodiodes responses to blue led's light ($\lambda = 490nm$) before and after gluing some of them on a thin plate of glass with epoxy glue (on average we measured a light transmission loss of 20%).

10) A typical ^{57}Co energy spectrum (central channel).

11) Noise correlation plot : the x-axis corresponds to the ^{57}Co determination (typical uncertainties : 5 to 10% , depending on the resolution and the background), the y-axis corresponds to the light and electric pulse test generators (uncertainties of 5% approximatively, mainly due the test capacitance uncertainty).

12) Raw correlation plots between the central channel (x-axis) and a neighbour (y-axis ; channel # 8) in ADC channel units :

12a) 6 Mev gamma line

12b) both 6 Mev and 14-17 Mev gamma lines

More than half of the total events populated the pedestals

13) Central crystal energy distribution : 6 Mev line

13a) raw spectrum

13b) with a 2 sigmas veto cut

13c) Pu-C source spectrum to be compared with figure 13a

14) Central crystal energy distribution : 14-17.6 Mev peaks

14a) raw spectrum

14b) with a two sigmas veto cut

14c) with a 0.5 sigma veto cut

15) Central crystal energy distribution : 6 Mev and 14-17 Mev peaks

15a) raw spectrum

15b) with a two sigmas veto cut

15c) with a 0.5 sigma veto cut

16) Central crystal energy distribution : 20 Mev line

16a) raw spectrum

16b) with a 2 sigma veto cut

16c) with a 0.5 sigma veto cut

17) Examples of HH^+ determination :

17a) gauss function

17b) "shower" function

18) Energy resolution of the central crystal versus energy : the resolution is defined here as Δ^+/peak for a two sigmas and a 0.5 sigma veto cut.

19) Example of simulated spectrum for a 20 Mev pure gamma ray without (full line) and with a 2 sigma veto cut (dotted line).

20) Experimental data versus Monte Carlo plot : the energy scale of the x-axis is given by the cosmic ray calibration ; the energy scale of the y-axis is given by EGS.

21) Energy sum distribution for the 20 Mev gamma :

21a) two highest channels summation

21b) 3 highest channels summation

21c) 4 highest channels summation

21d) 5 highest channels summation

22) Energy resolution (Δ^+/peak) as a function of the highest energy crystals number. For the central crystal (#1) , the three points correspond to different veto energy cut-off (0.5 σ , 1 σ and 2 σ).

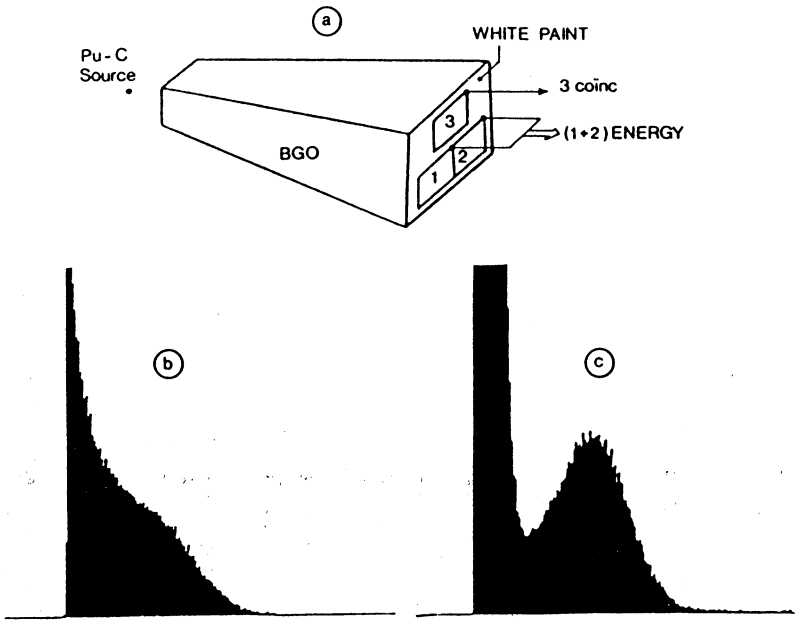

Figure 1

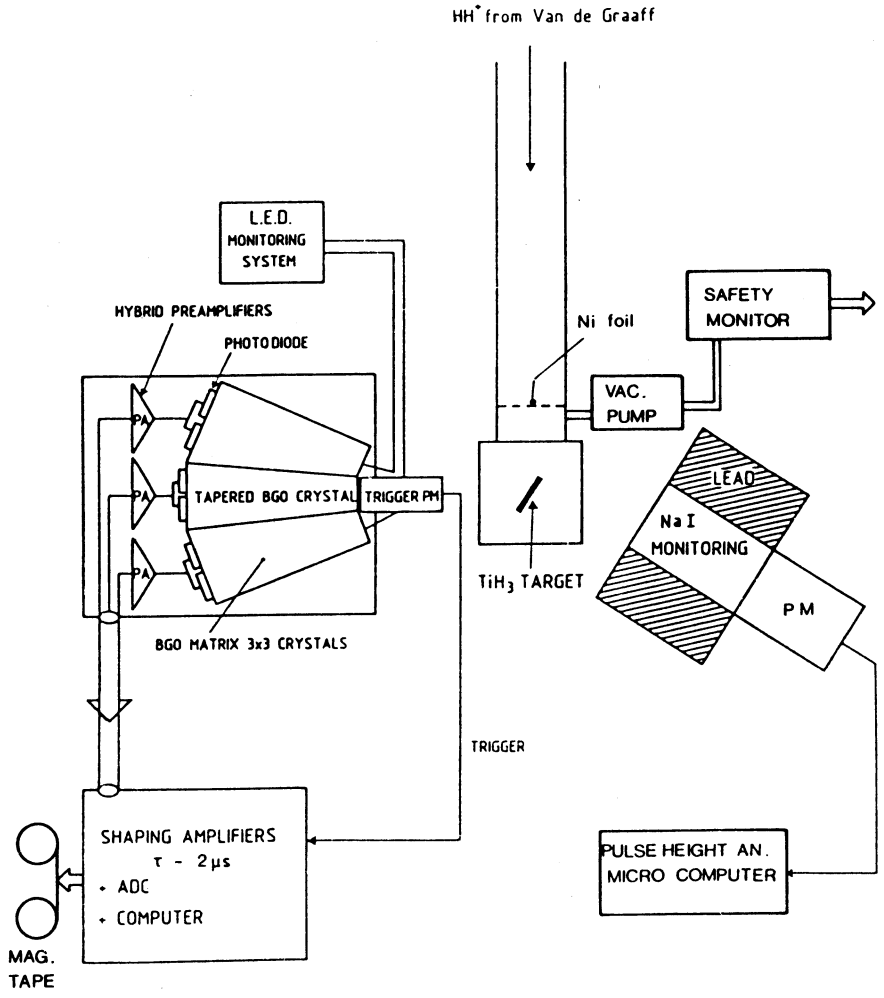

LAYOUT OF THE VAN DE GRAAFF EXPERIMENT.

Figure 2

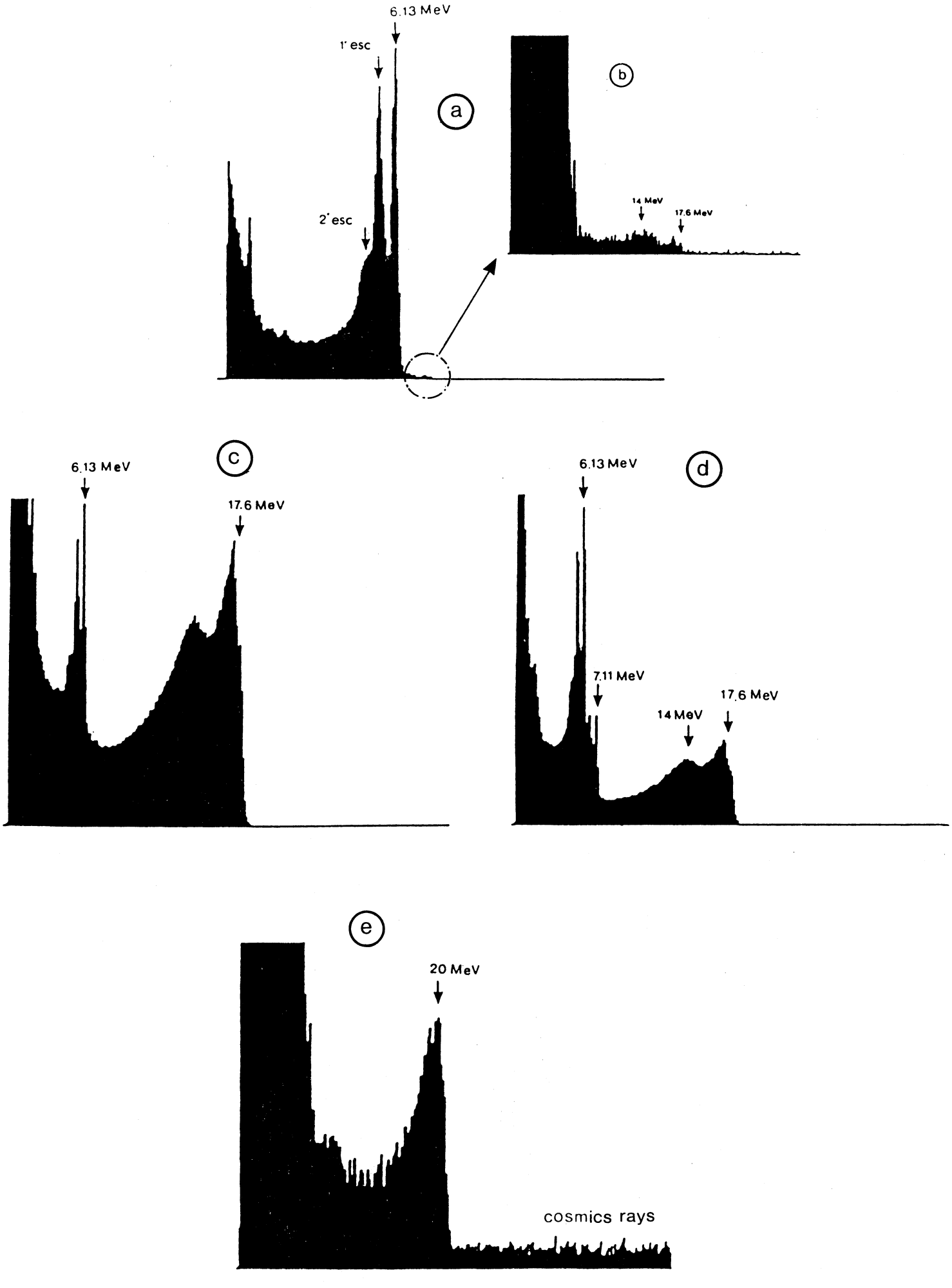
6.13 MeV
1° esc
2° esc
a
b
14 MeV
17.6 MeV
c
6.13 MeV
17.6 MeV
d
6.13 MeV
7.11 MeV
14 MeV
17.6 MeV
e
20 MeV
cosmics rays

Figure 3

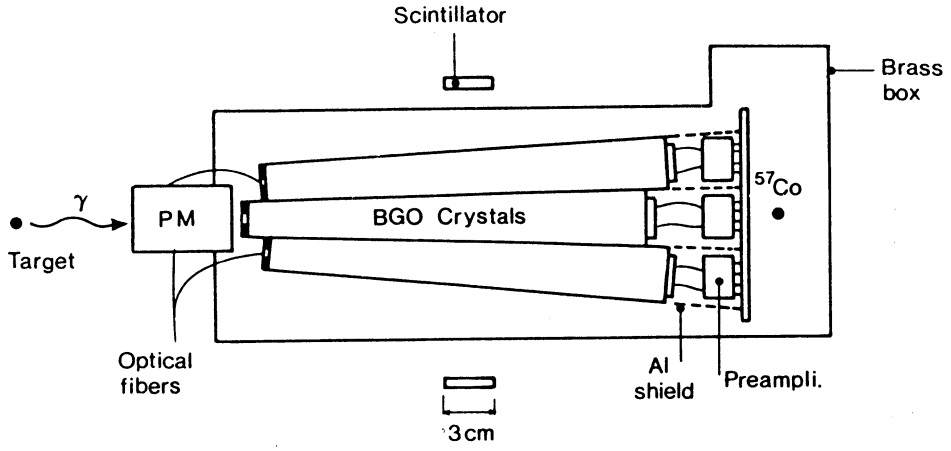

Figure 4

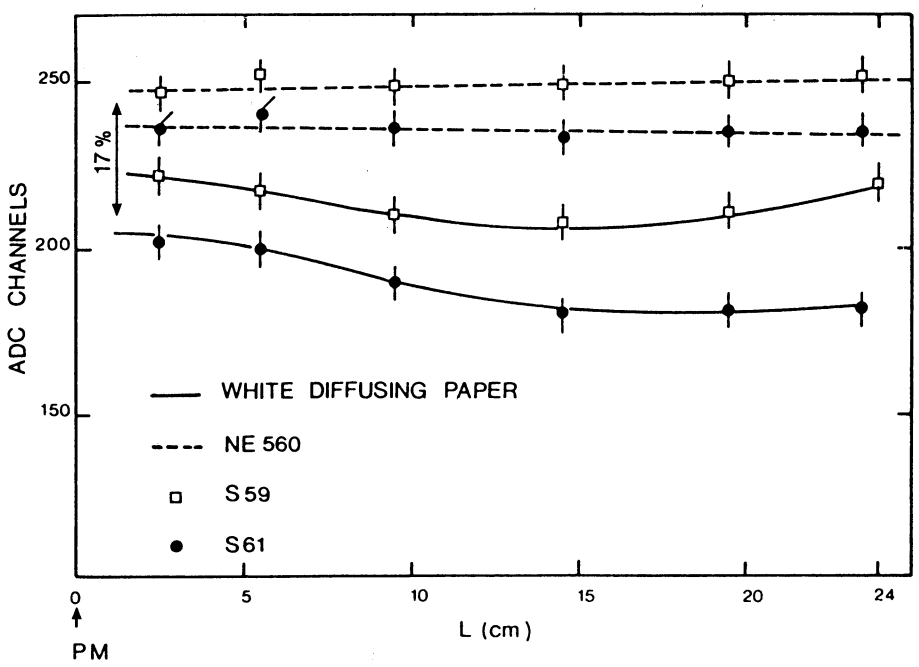

Figure 5

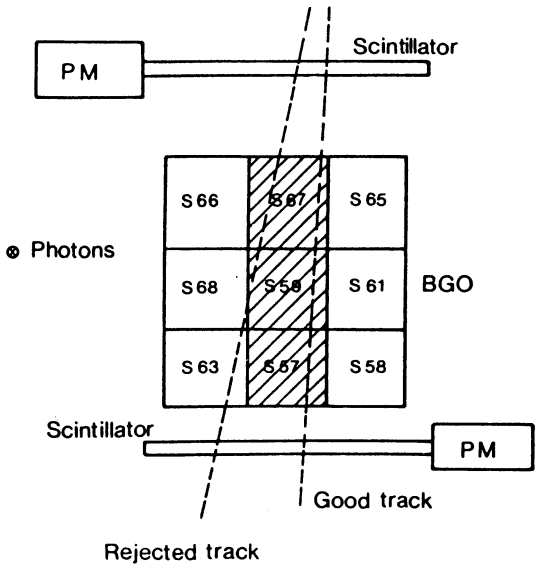

Figure 6

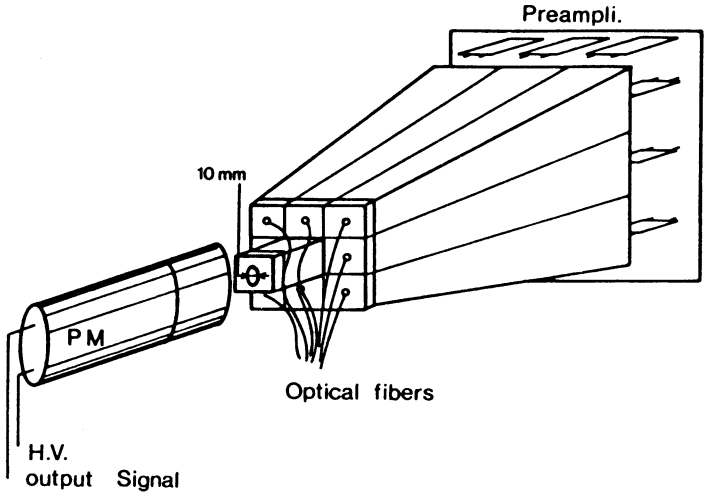

Figure 7

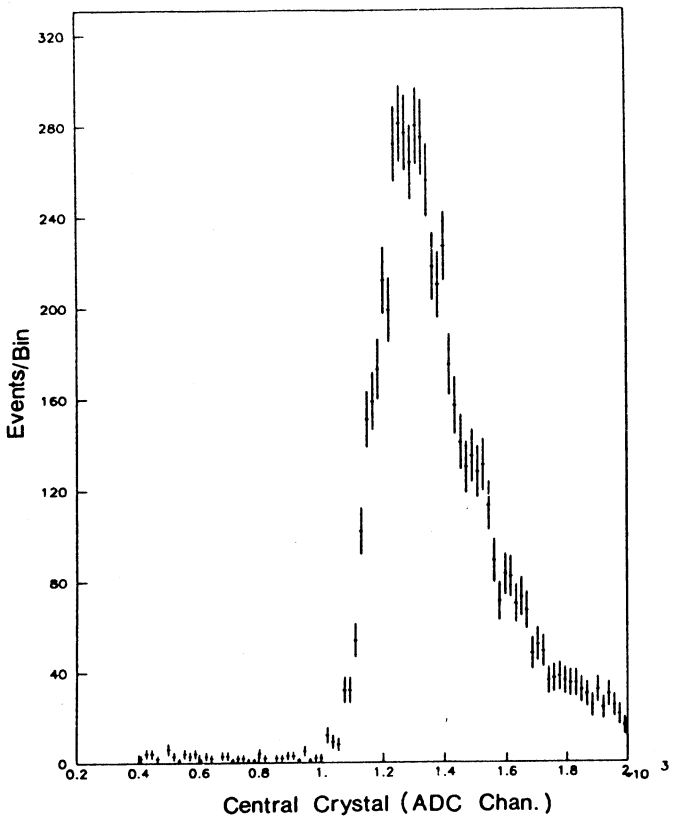

Figure 8

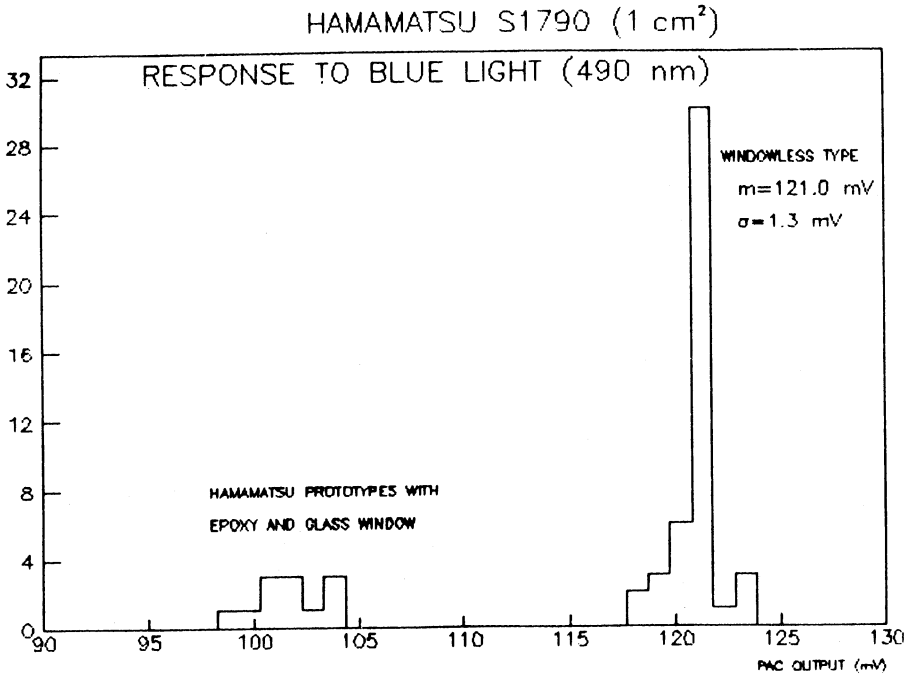

Figure 9

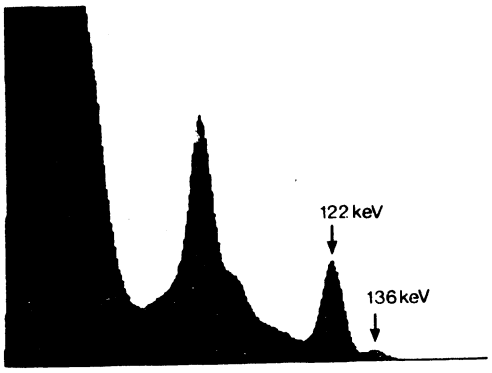

Figure 10

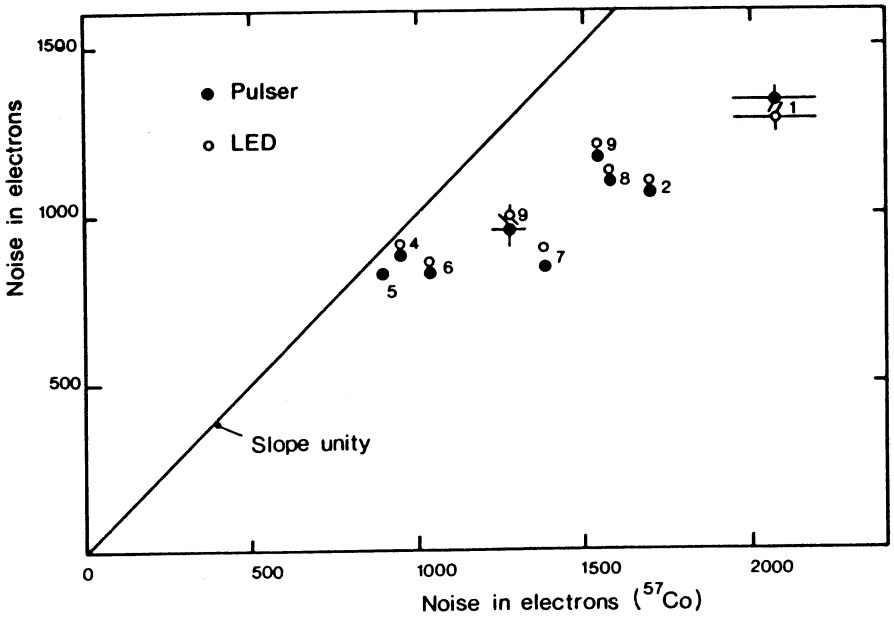

Figure 11

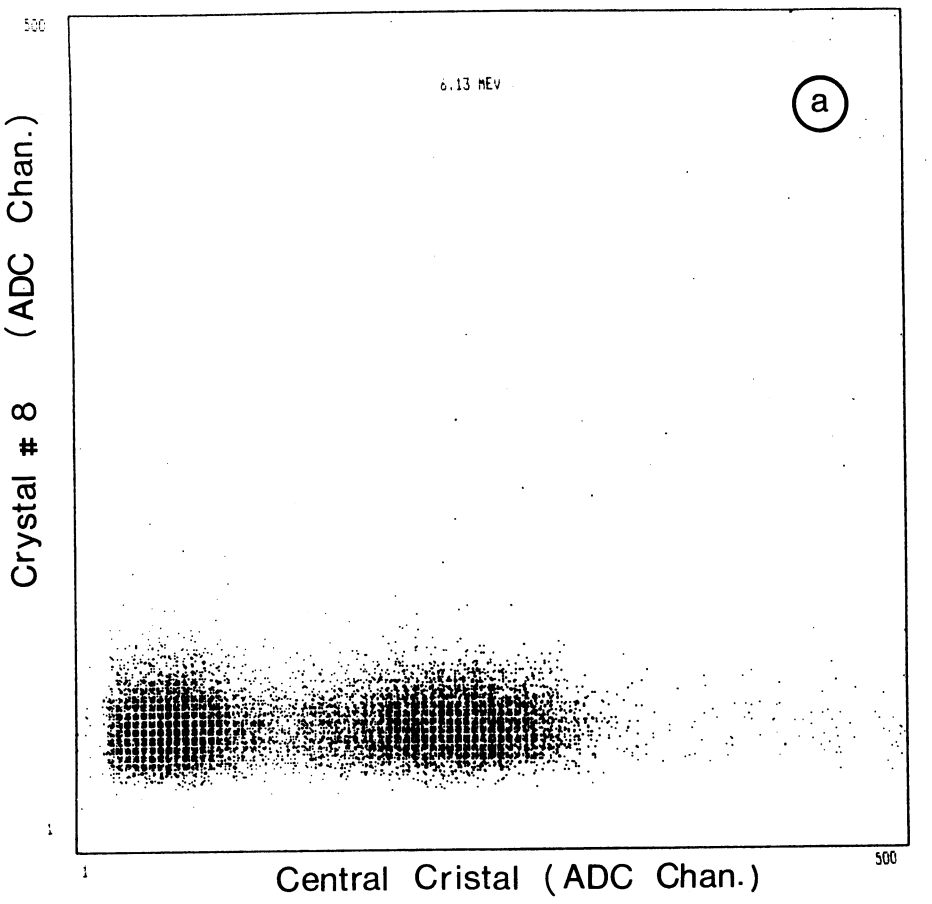
500
6.13 MEV
a
Crystal # 8 (ADC Chan.)
1
1
500
Central Cristal (ADC Chan.)

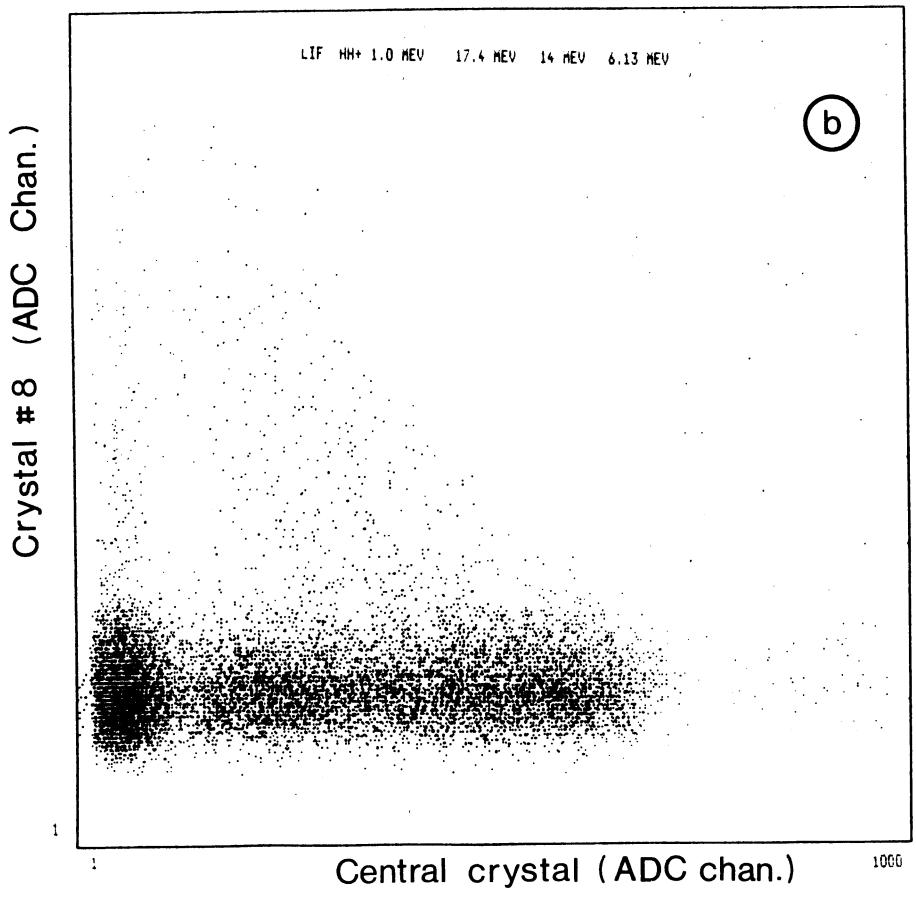
LIF HH+ 1.0 MEV 17.4 MEV 14 MEV 6.13 MEV
b
Crystal #8 (ADC Chan.)
1
1
1000
Central crystal (ADC chan.)

Figure 12

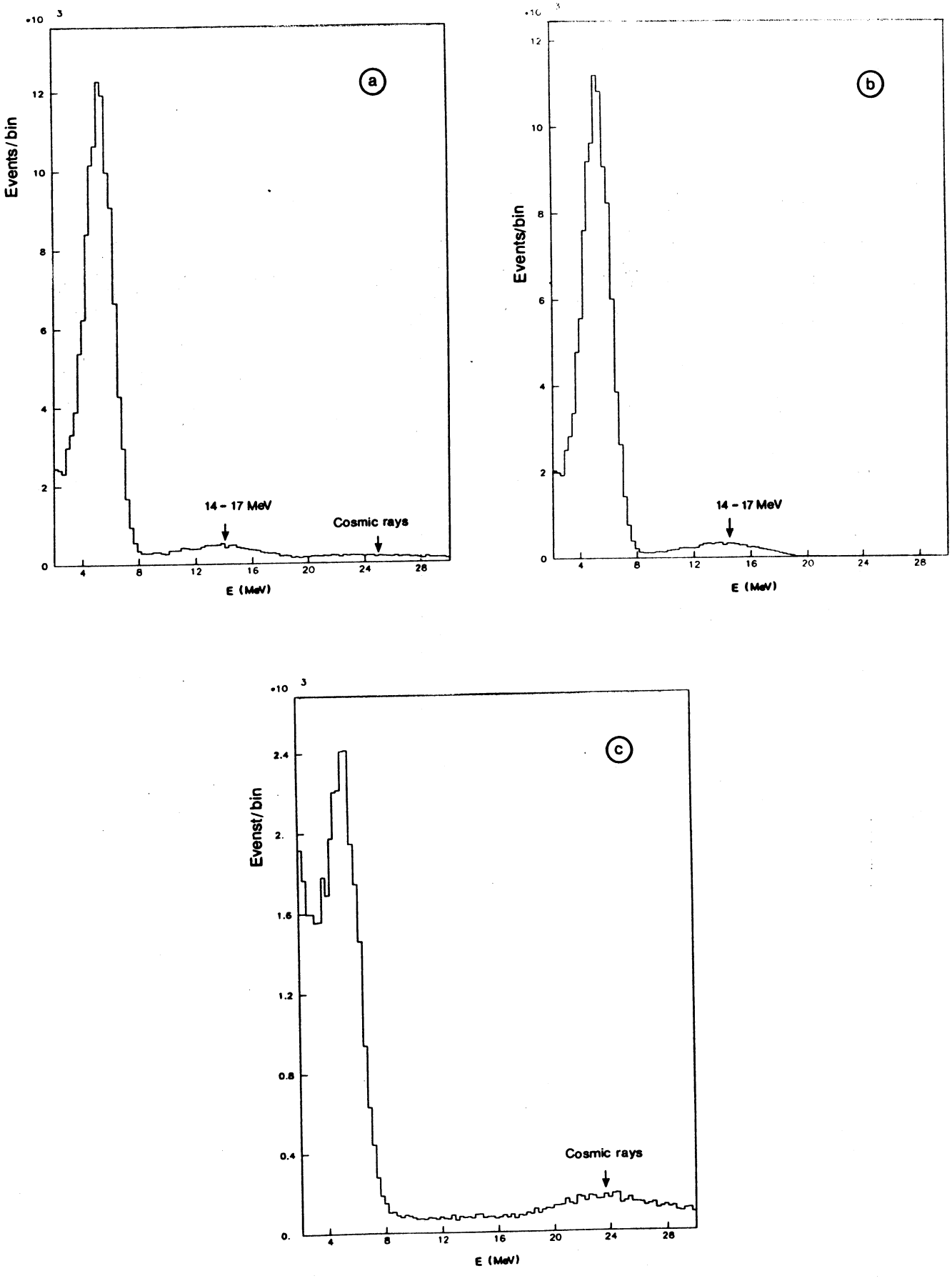
a
Events/bin
E (MeV)
14 - 17 MeV
Cosmic rays
b
Events/bin
E (MeV)
14 - 17 MeV
c
Evenst/bin
E (MeV)
Cosmic rays

Figure 13

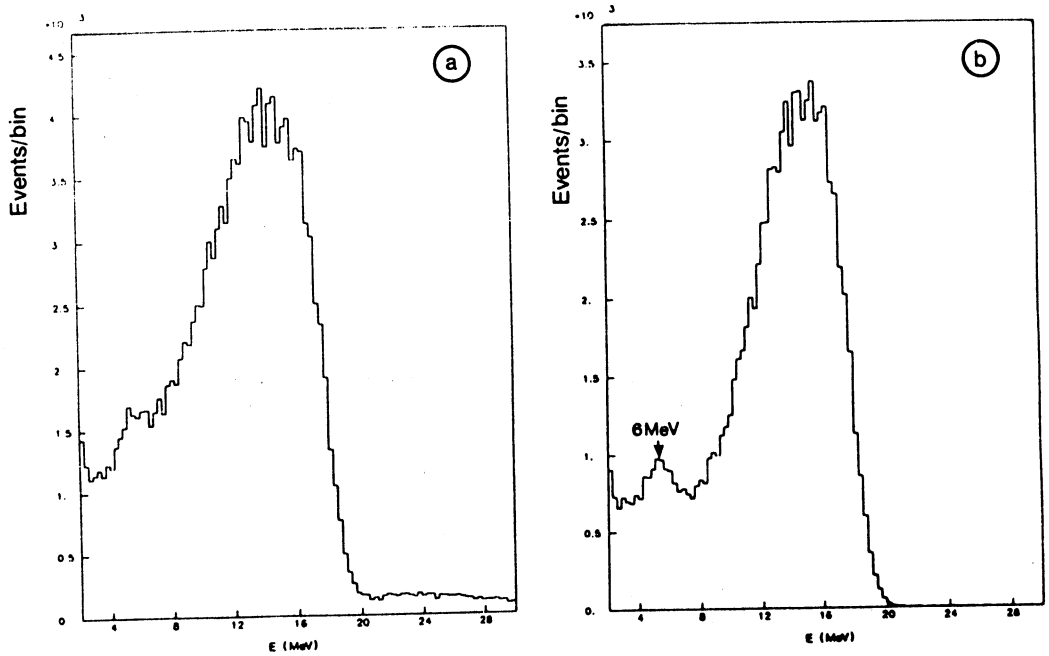

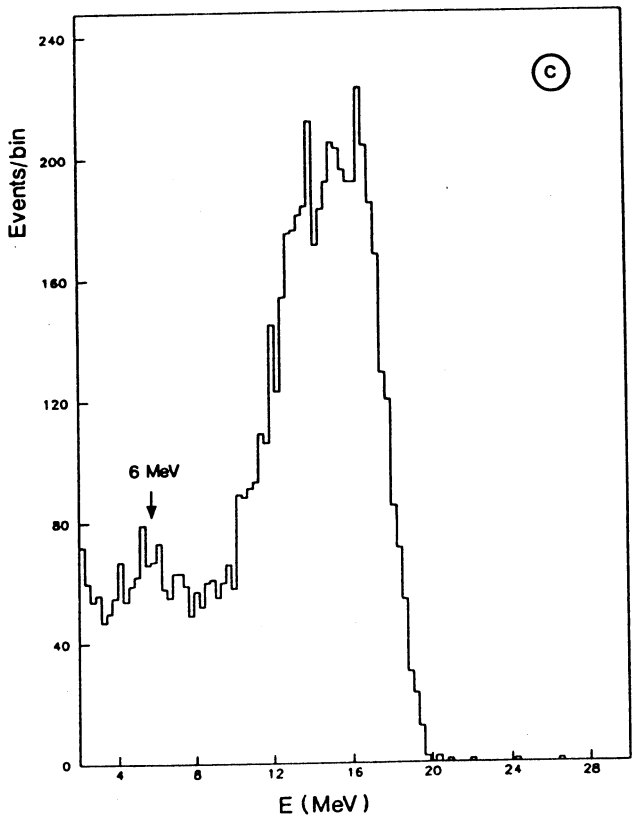

Figure 14

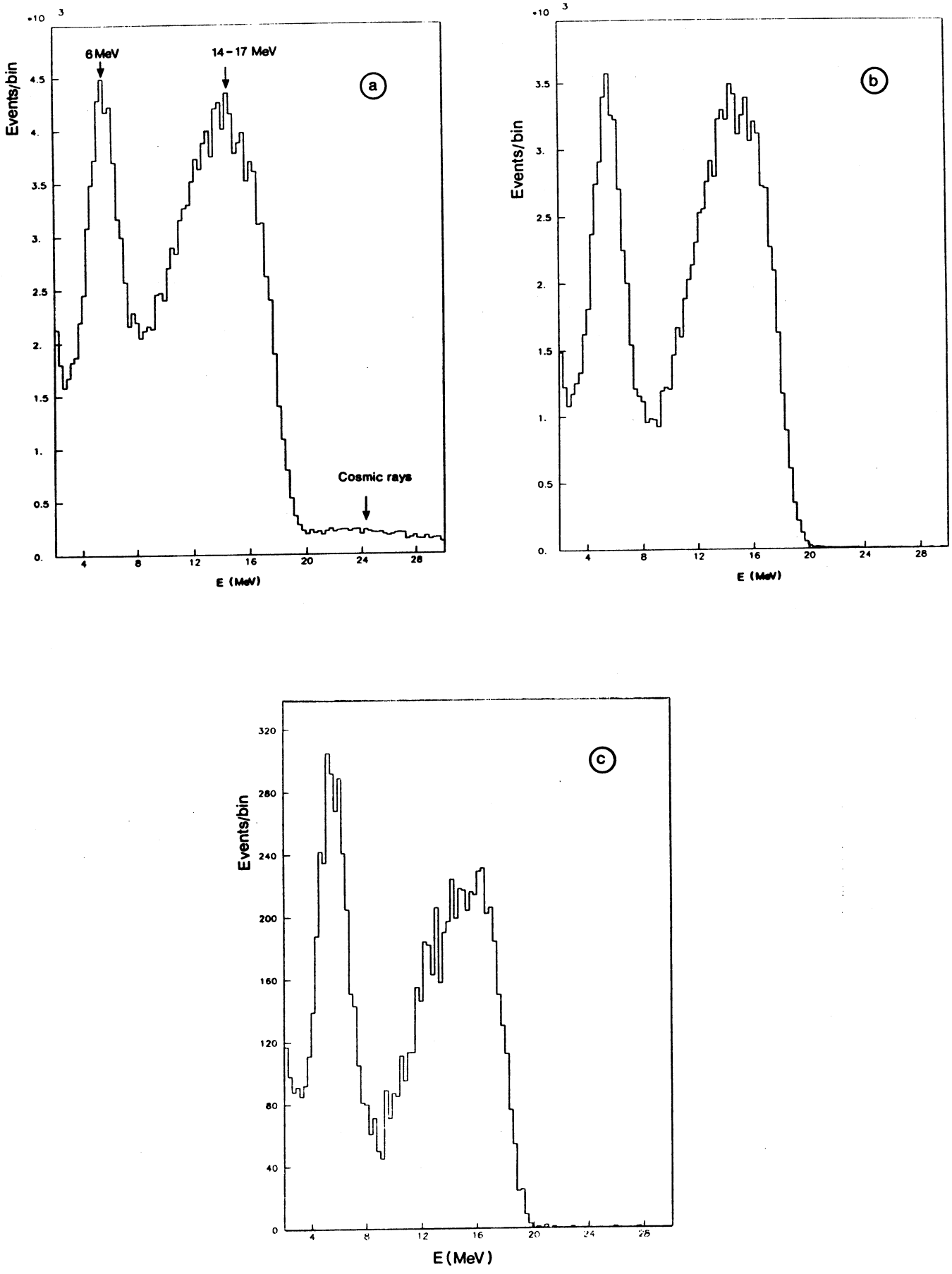

Figure 15

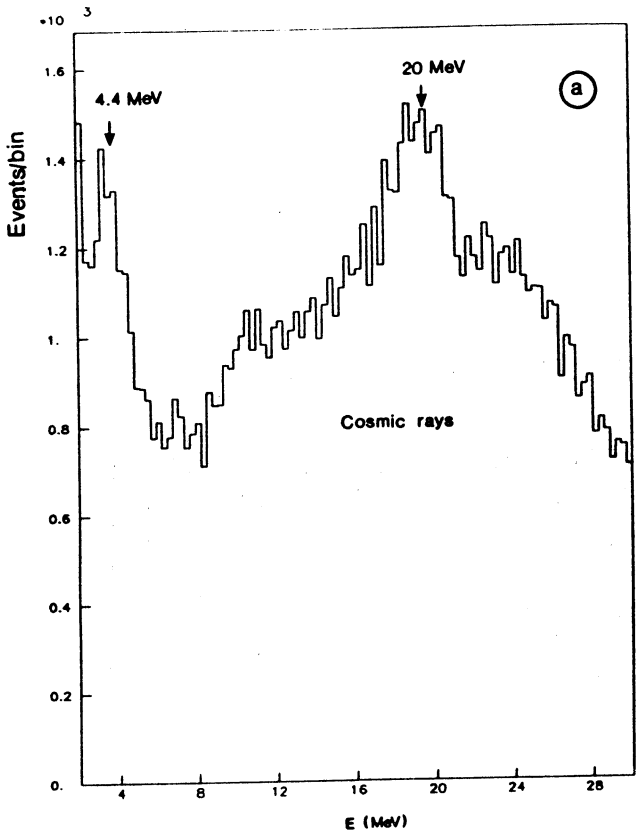
a
4.4 MeV
20 MeV
Cosmic rays
Events/bin
E (MeV)

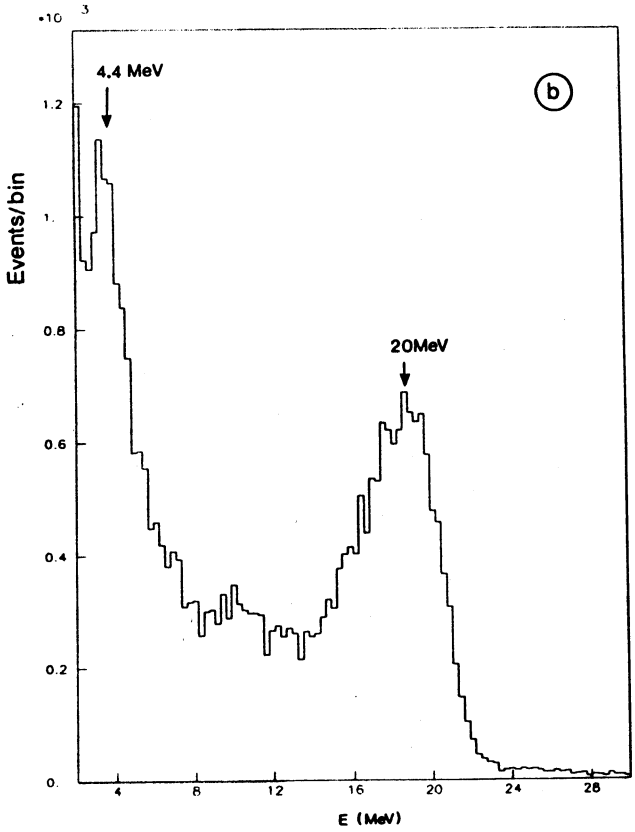
b
4.4 MeV
20MeV
Events/bin
E (MeV)

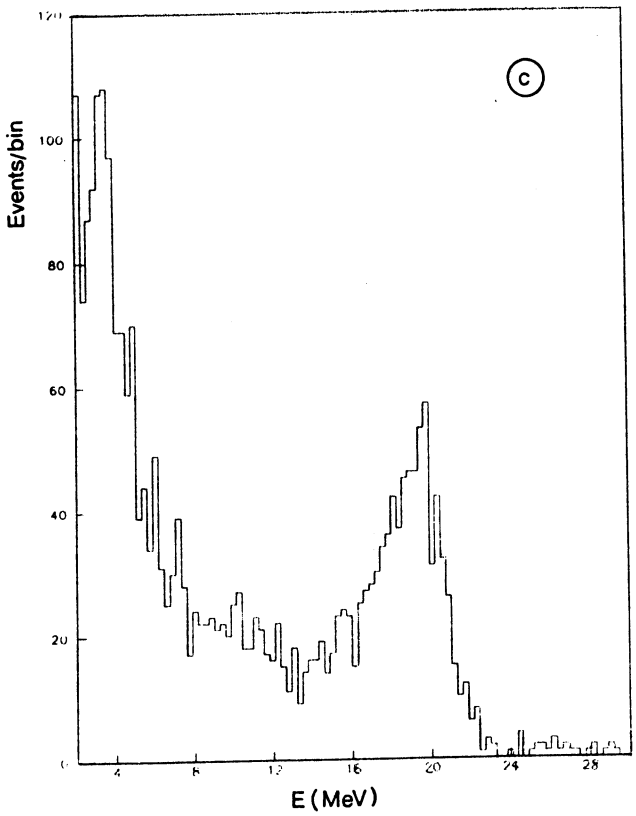
c
Events/bin
E (MeV)

Figure 16

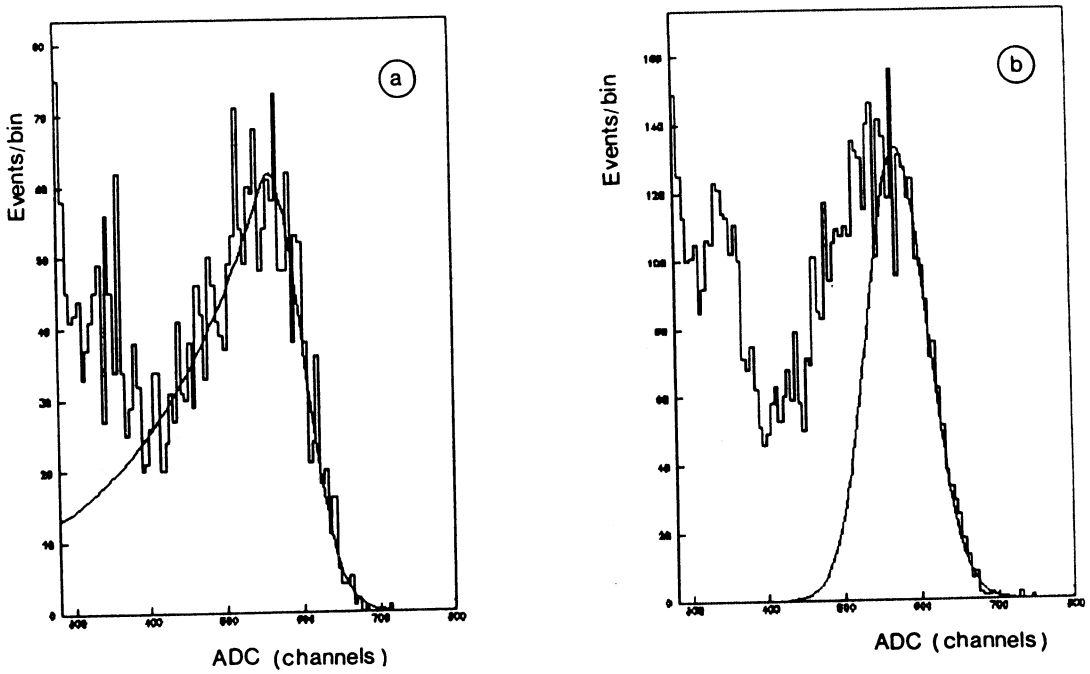

Figure 17

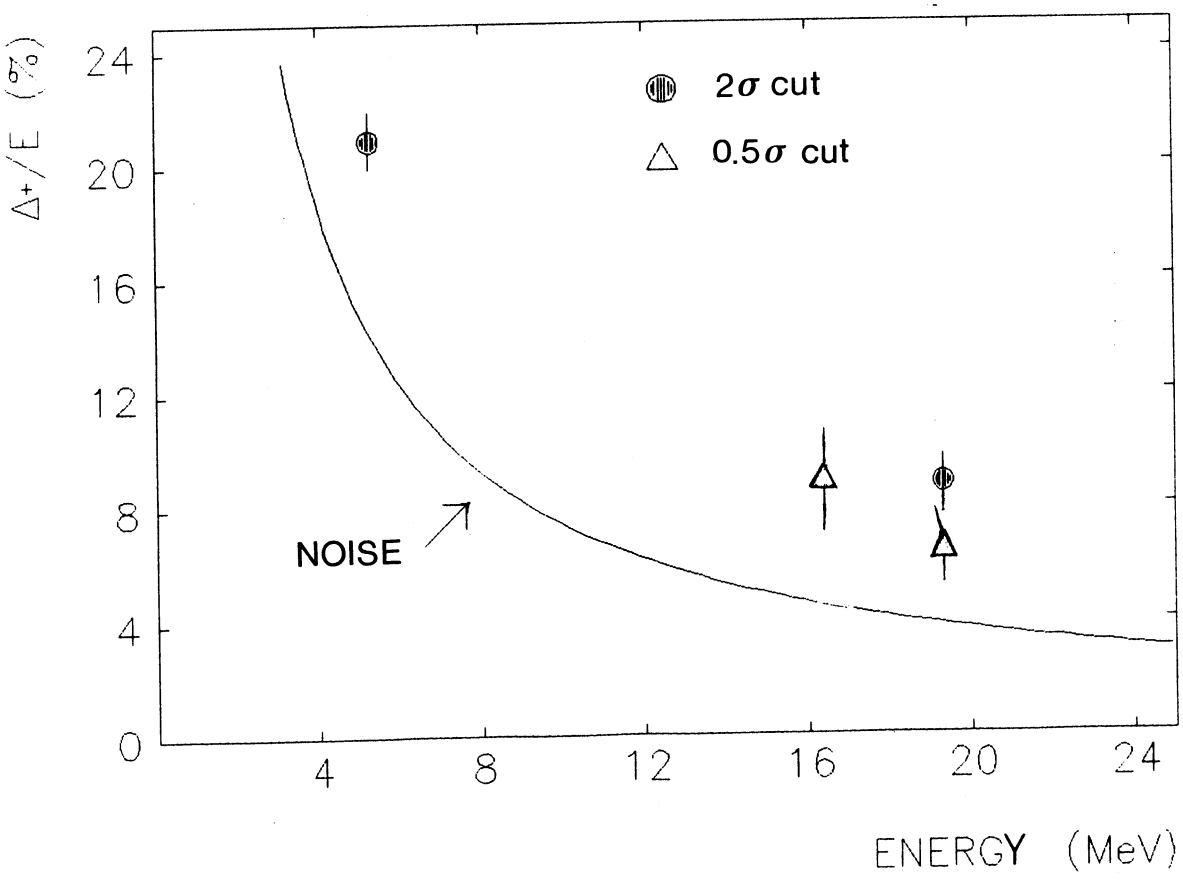

Figure 18

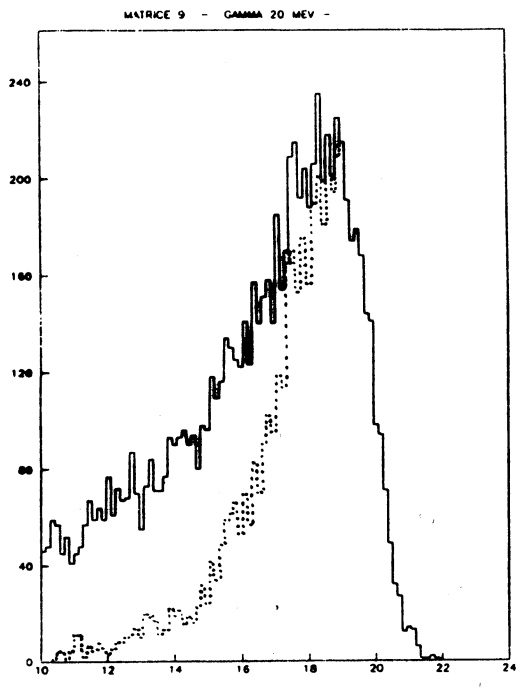

Figure 19

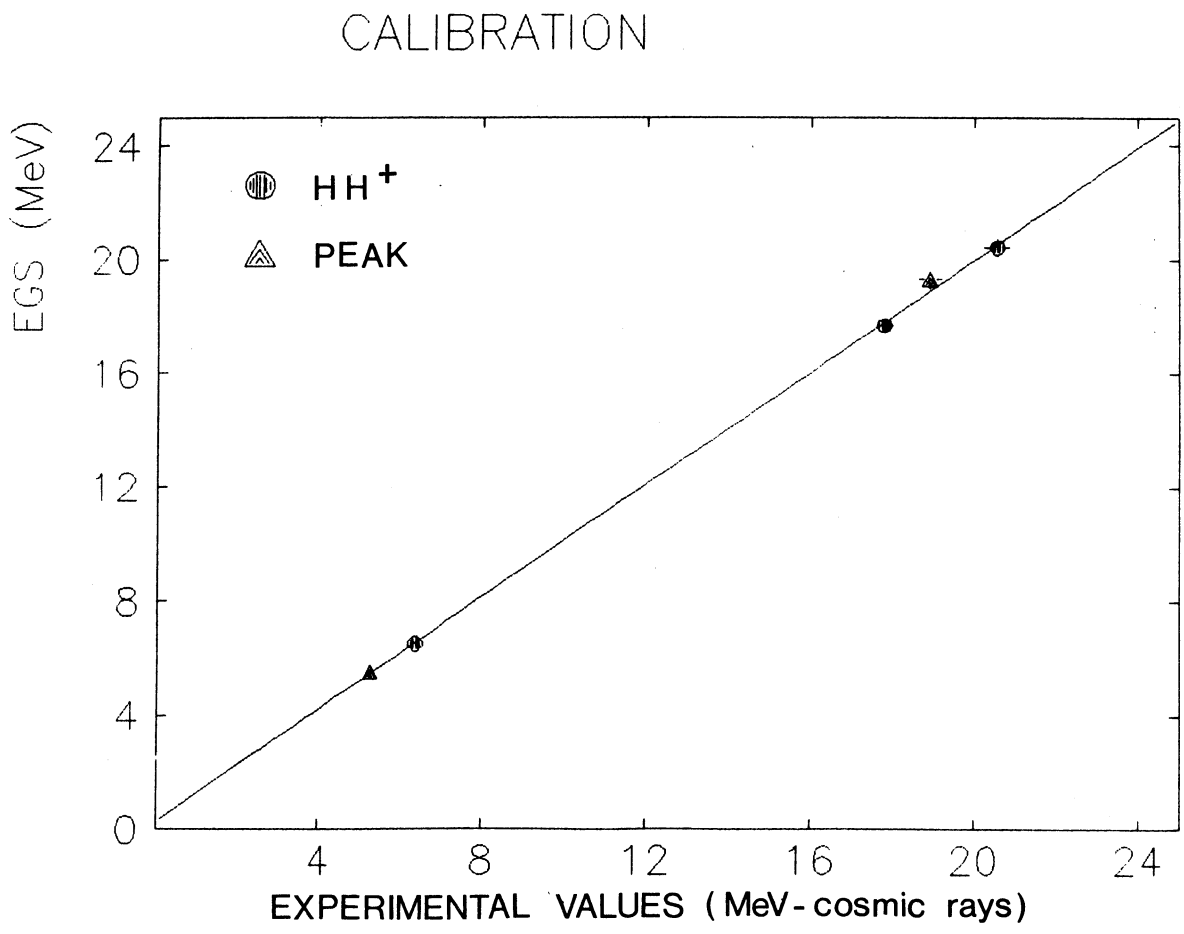

Figure 20

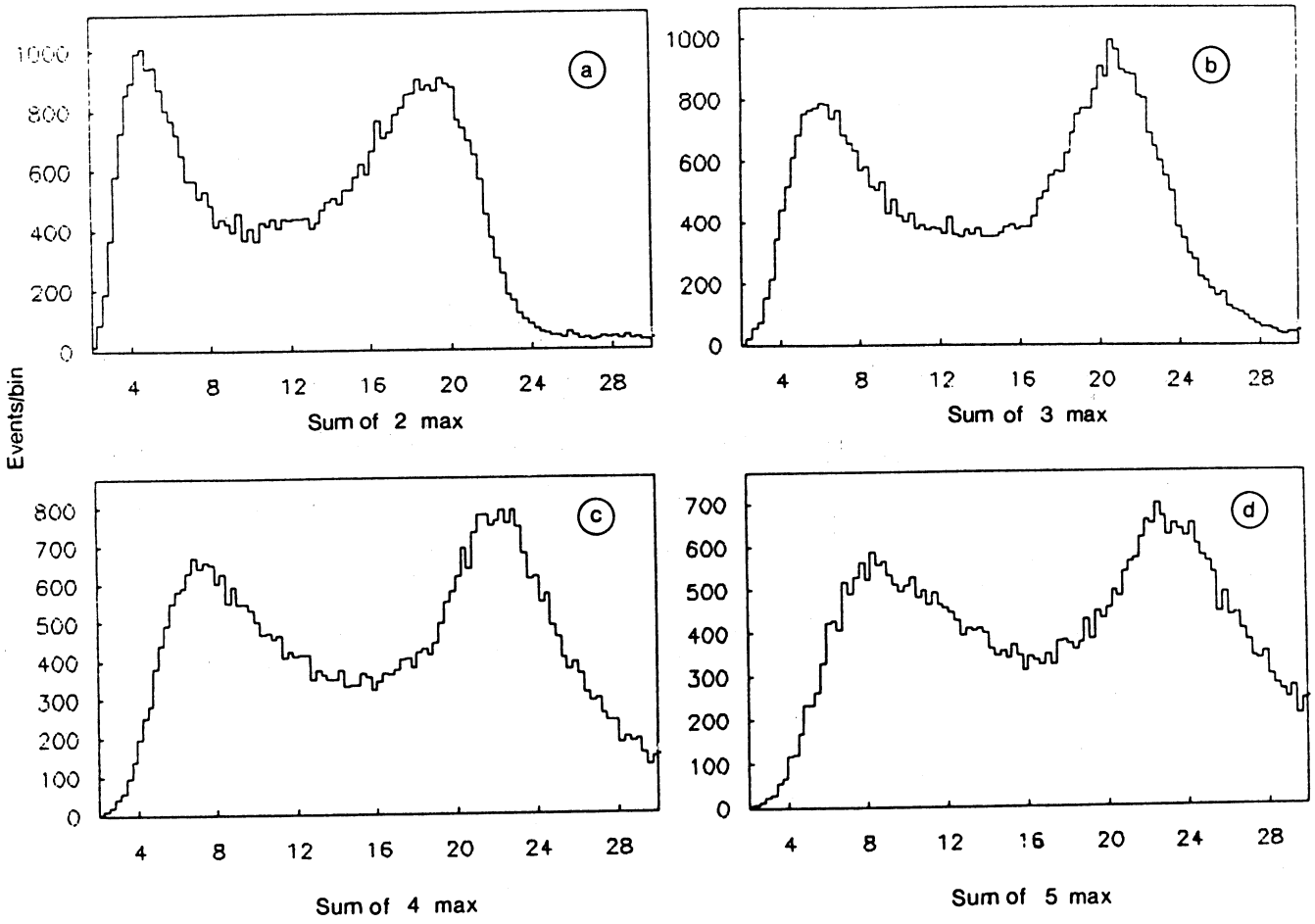

Figure 21

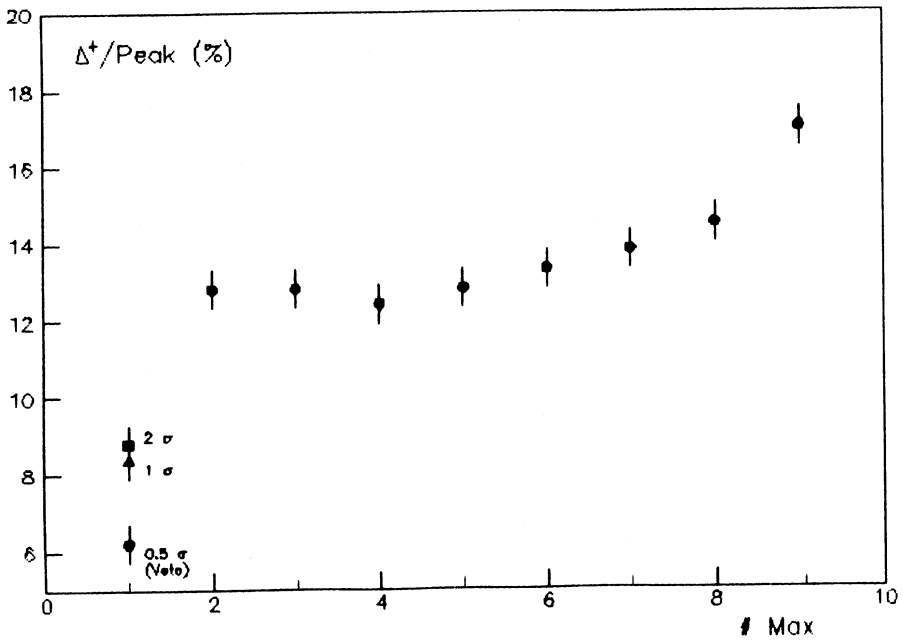

Figure 22